Supplementary Information

Post-Synthetic Gridization Enhances Spin-Flip Dynamics, Horizontal Alignment, and Ozone Resistance in Solution-Processable TADF Macrocycles

Quanyou Feng,[a]# Aiyun Zhu,[a]# Qiuhu Han,[a] Kewei Guo,[a] Yunfei Zhu,[a] Yue Cao,[a] Jingyao Ma,[a] Hao Li,[a] Hongjian Wang,[a] Yuyu Pan,[b]* Xinxin Ban,[c] Mengna Yu,[a] Man Xu,[a] Zilu Wang,[a]* Guohua Xie,[d] Linghai Xie[a,e]*, Wei Huang[a,e,f]*

[a] Centre for Molecular Systems and Organic Devices (CMSOD), State Key Laboratory of Flexible Electronics, Institute of Advanced Materials (IAM), Nanjing University of Posts & Telecommunications, 9 Wenyuan Road, Nanjing 210023, P. R. China

[b] School of Petrochemical Engineering, Shenyang University of Technology, 30 Guanghua Street, Liaoyang 111003, P. R. China

[c] School of Environmental and Chemical Engineering, Jiangsu Key Laboratory of Function Control Technology for Advanced Materials, Jiangsu Ocean University, 59 Cangwu Road, Lianyungang 222005, P. R. China

[d] The Institute of Flexible Electronics (Future Technologies), Xiamen University, 422 Siming South Road, Xiamen 361005, P. R. China

[e] School of Flexible Electronics (SoFE) and Henan Institute of Flexible Electronics (HIFE), Henan University, 379 Mingli Road, Zhengzhou 450046, P. R. China

[f] Frontiers Science Center for Flexible Electronics (FSCFE), State Key Laboratory of Flexible Electronics, Northwestern Polytechnical University, 127 West Youyi Road, Xi'an 710072, China

*Corresponding Authors: vc@nwpu.edu.cn (Wei Huang); iamlhxie@njupt.edu.cn (Linghai Xie); panyu0422@sut.edu.cn (Yuyu Pan); iamzlwang@njupt.edu.cn (Zilu Wang)

# Q.F. and A.Z. contributed equally.

Contents

S1. Experimental section

Materials and methods

All the reagents and solvents were commercially available and used without further purification. Tetrahydrofuran (THF) was dried over sodium benzophenone ketyl anion radical and distilled under a dry nitrogen atmosphere immediately prior to use. Other solvents were distilled under a dry nitrogen atmosphere immediately prior to use. The emitter phenoxazine–triphenyltriazine (PXZ-TRZ) was synthesized according to the literature procedure.[1] The (DOHSBF) was synthesized according to our previous work.[2] The ^{1}H and ^{13}C NMR spectra were recorded on a Bruker Avance spectrometer (400 MHz) in $CDCl_3$ with tetramethylsilane (TMS) as the internal standard at 298 K. MALDI-TOF mass spectra were performed on a Bruker BIFLEX III ultrahigh-resolution Fourier transform ion cyclotron resonance (FT-ICR) mass spectrometer.

UV/Vis absorption spectra were measured by a shimadzu UV-3600 spectrometer at 298 K. The absorption spectra was performed on some solution (10^{-5}M). Photoluminescence spectra were recorded on a shimadzu RF-5301(PC) luminescence spectrometer. Phosphorescence spectra was characterized to obtain Triplet energy values of the TADF materials at 77 K. Photoluminescence quantum yield (PLQY) was obtained using an integrating sphere (C992002, Hamamatsu Photonics Co., Japan) with a Xe lamp as the excitation source and a multichannel spectrometer (Hamamatsu PMA-11) as the optical detector. The PL transient decay curves of the films were measured using a transient spectrometer (Edinburg FLS920) with a picosecond pulsed UV-LASTER (λ = 379 nm, pulse width = 89 ps) as the excitation source. The dipole orientation of the doped film was determined by R1-OLED Angular Resolution spectrometer. A doped film with a thickness of 50 nm was deposited onto a fused-silica-based half-cylindrical lens. A continuous-wave He:Cd laser (375 nm) with a fixed angle of 45° to the substrate was employed as the excitation source. The p-polarized emission light was detected at the PL peak wavelength of the dopants.

Cyclic voltammetric studies were measured by using an CHI660C Electrochemical Workstation in a typical three-electrode consisting of a platinum sheet working

electrode, a silver/silver nitrate (Ag/Ag^{+}) reference electrode and a platinum wire counter electrode. Ferrocene was used as the internal standard reference for each measurement. All electrochemical experiments were carried out under a nitrogen atmosphere at room temperature in an electrolyte solution of 0.1 M tetrabutylammonium hexafluorophosphate (n-Bu_4NPF_6) in anhydrous CH_2Cl_2 with a scan rate of 100 mV s^{-1}. The HOMO energy levels were calculated according to the equation $E_{HOMO} = -(E_{onset}^{ox} + 4.8)$ ev, where E_{onset}^{ox} was the onset of the oxidation potential. The LUMO energy levels were determined from E_{HOMO} and Energy level gaps (E_g), where E_g was derived from the onset of the absorption spectra.

TGA were conducted by a Shimadzu DTG-60H under a heating rate of 10 ℃ min^{-1} and a nitrogen flow rate of 50 cm^3 min^{-1}. DSC measurement result was obtained by using a Shimadzu Instruments DSC60A. DSC data were collected from 30 to 300 ℃ at a rate of 10 ℃ min^{-1} for both of the baseline and sample.

All computational analyses were conducted utilizing the Gaussian 09. The ground state geometries were refined through Density Functional Theory (DFT) calculations employing the M062X functional with a 6-31G* basis set. Subsequently, Time-Dependent Density Functional Theory (TD-DFT) calculations were executed for the excited state utilizing the M062X functional too. These calculations were based on the optimized geometries of the lowest singlet and triplet states. Furthermore, the root mean square displacement (RMSD) between the ground and excited state geometries and the analysis of the natural transition orbitals (NTOs) were performed using Multiwfn version 3.8.

Devices were fabricated by vacuum deposition onto pre-coated ITO glass substrates with sheet resistance of 15 Ω/square at a pressure lower than 1×10^{-4} mbar for organic and metal deposition. Before the fabrication of devices, the ITO glass substrates were cleaned with Decon 90, rinsed in ultrapure water and ethanol, dried in an oven at 120 °C, by plasma cleaning process. Then 30 nm PEDOT:PSS was spin-coated onto the ITO substrate and dried at 200 ℃ for 10 min. The substrates were then taken into a nitrogen glove box, where the 40 nm emission layer was spin coated onto the PEDOT:PSS layer from chlorobenzene and annealed at 100 ℃ for 30 min. After that, 40 nm TPBI was

vacuum-deposited as the electron transporting layer. Cs_2CO_3 and Al were subsquently deposited as the cathode at a deposition rate of 0.1 Å s^{-1} and 5 Å s^{-1}, respectively. EL spectra and CIE color coordinates were measured with a Spectrascan PR650 photometer, and the current-voltage characteristics were measured with a computer-controlled Keithley 2400 Source Meter under ambient atmosphere.

Analysis of Rate Constants[3]

The lifetime τ_p and τ_d represent the prompt and decay fluorescence lifetime, which determined from transient PL spectra following below two equations:

$$R(t) = A_1 e^{(-\tau/\tau_1)} + A_2 e^{(-\tau/\tau_2)} + A_3 e^{(-\tau/\tau_3)} \qquad \text{Eq. (1)}$$

$$\tau_{av} = \frac{\sum A_i \tau_i^2}{A_i \tau_i} \qquad \text{Eq. (2)}$$

Where R(t) is the fited function of the measured transient PL decay spectra, A_i is the pre-exponential for lifetime τ_i, the average lifetime τ_{av} is calculated from Eq.(2). The rate constants of radiative decay ($k_{r,S}$) and nonradiative decay ($k_{nr,S}$) from S_1 to S_0 states, the reverse intersystem crossing (k_{RISC}) were calculated from the following five equations:

$$k_p = \frac{1}{\tau_p} \qquad \text{Eq. (3)}$$

$$k_d = \frac{1}{\tau_d} \qquad \text{Eq. (4)}$$

$$k_{r,s} = \emptyset_{PF} k_p + \emptyset_{DF} k_d \approx \emptyset_{PF} k_p \qquad \text{Eq. (5)}$$

$$k_{nr,s} = \frac{1-PLQY}{PLQY} k_{r,s} \qquad \text{Eq. (6)}$$

$$k_{RISC} = \frac{k_p k_d PLQY}{k_{r,s}} \qquad \text{Eq. (7)}$$

Where the k_p and k_d represent the decay rate constants for prompt and delayed fluorescence, respectively. Φ_{PF} and Φ_{DF} indicate prompt and delayed fluorescence components and can be distinguished from the total PLQY by comparing the integrated intensities of prompt and delayed components in the transient PL spectra.

For further simplifying the calculations, the Eq. (7) can be simplified as following:

$$k_{RISC} = \frac{PLQY}{\tau_d \emptyset_{PF}} \qquad \text{Eq. (8)}$$

Scheme S1. Straightforward synthetic route to AG-EtPXZ.

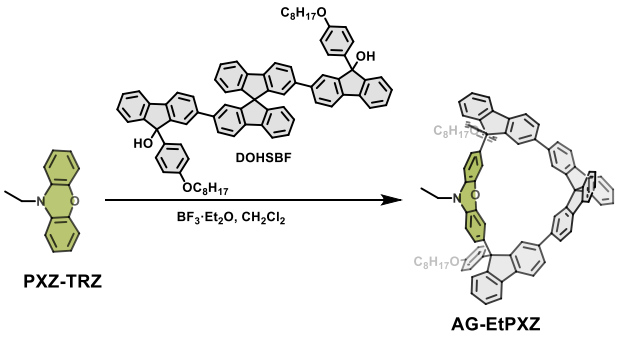

In a 500 mL two-necked round-bottomed flask charged with EtPXZ (0.17 g，0.82 mmol) and DOHSBF (0.88 g，0.82 mmol) in 250 mL of dry dichloromethane, a solution of $BF_3{\cdot}Et_2O$ (0.20 g，0.2 mL) in 50 mL dry dichloromethane was added dropwise. The reaction mixture was stirred at room temperature for 12 h. Water (100 mL) was added to quench the reaction. The mixture was separated and the aqueous phase was extracted with dichloromethane. The combined organic layers were washed with brine and dried over $MgSO_4$. After removal of the solvent, the crude product was purified by flash column chromatography using an eluent of petroleum ether: dichloromethane (4:1) to give a light yellow solid product AG-EtPXZ (0.10 g，10%). 1H NMR (400 MHz, $CDCl_3$) δ 7.83 (t, J = 7.6 Hz, 1H), 7.77-7.52 (m, 8H), 7.47-7.31 (m, 4H), 7.24-7.06 (m, 9H), 7.05-6.79 (m, 11H), 6.71-6.46 (m, 9H), 4.00-3.47 (m, 6H), 1.24-1.05 (m, 23H), 0.77 (dq, J = 11.9, 7.7, 7.1 Hz, 10H). MALDI-TOF-MS: m/z calcd for $C_{93}H_{81}NO_3$ $[M]^+$:1259.62, found：1259.33.

Scheme S2. Straightforward synthetic route to AG-PXZ-TRZ.

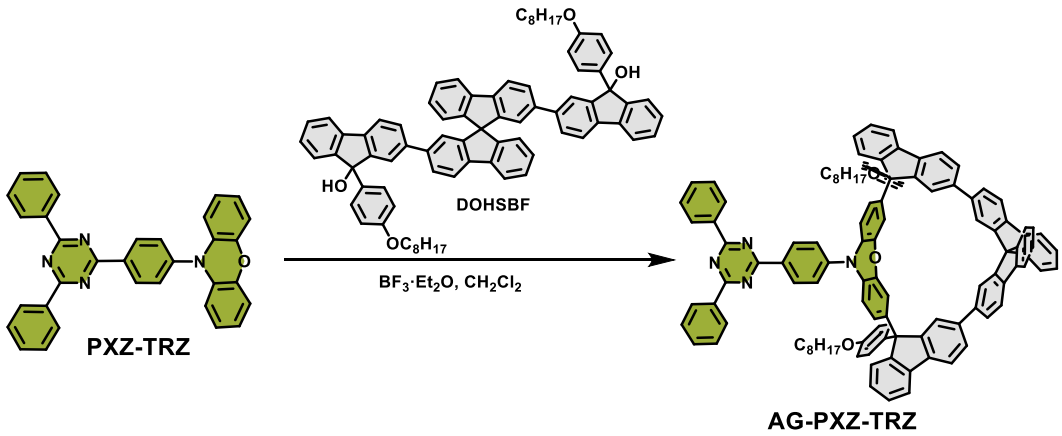

In a 500 mL two-necked round-bottomed flask charged with PXZ-TRZ (0.40 g，0.82 mmol), DOHSBF (0.88 g，0.82 mmol) and 250 mL of dry dichloromethane, a solution of $BF_3 \cdot Et_2O$ (0.20 g，0.2 mL) in 50 mL dry dichloromethane was added dropwise. The reaction mixture was stirred at room temperature for 12 h. Water (100 mL) was added to quench the reaction. The mixture was separated and the aqueous phase was extracted with dichloromethane. The combined organic layers were washed with brine and dried over $MgSO_4$. After removal of the solvent, the crude product was purified by flash column chromatography using an eluent of petroleum ether: dichloromethane (4:1) to give a light yellow solid product AG-PXZ-TRZ (1.06 g，84%). ^{1}H NMR (400 MHz, $CDCl_3$) δ 8.93-8.72 (m, 7H), 8.05-7.84 (m, 4H), 7.81-7.62 (m, 4H), 7.60 (ddd, *J* = 14.3, 7.3, 3.6 Hz, 9H), 7.44 (t, *J* = 8.2 Hz, 3H), 7.35 (td, *J* = 13.4, 11.1, 6.2 Hz, 4H), 7.29-7.17 (m, 4H), 7.17 (dt, *J* = 9.4, 4.8 Hz, 4H), 7.10-6.94 (m, 5H), 6.93-6.61 (m, 9H), 6.59 (s, 10H), 3.92 (ddt, *J* = 31.1, 27.3, 6.4 Hz, 4H), 1.77 (s, 3H), 1.49-1.27 (m, 42H), 1.11 (s, 22H), 0.94 (ddd, *J* = 14.1, 6.6, 3.4 Hz, 9H), 0.92-0.85 (m, 9H), 0.11 (s, 8H), 0.06 (s, 6H). ^{13}C NMR (101 MHz, $CDCl_3$) δ 171.75, 170.07, 152.74, 150.83, 149.82, 139.76, 136.04, 132.65, 130.55, 129.92, 129.00, 128.71, 127.85, 127.07, 126.74, 123.66, 120.68, 120.37, 120.09, 119.94, 118.58, 115.62, 114.06, 113.35, 85.36, 81.58, 74.45, 67.93, 64.29, 45.47, 37.41, 31.96, 31.83, 29.73, 29.30, 26.10, 22.72, 14.16, 1.05, 0.03. MALDI-TOF-MS: m/z calcd for $C_{112}H_{90}N_4O_3$ $[M]^+$:1539.705, found: 1539.274.

Scheme S3. Straightforward synthetic route to DSFPXZ-TRZ.

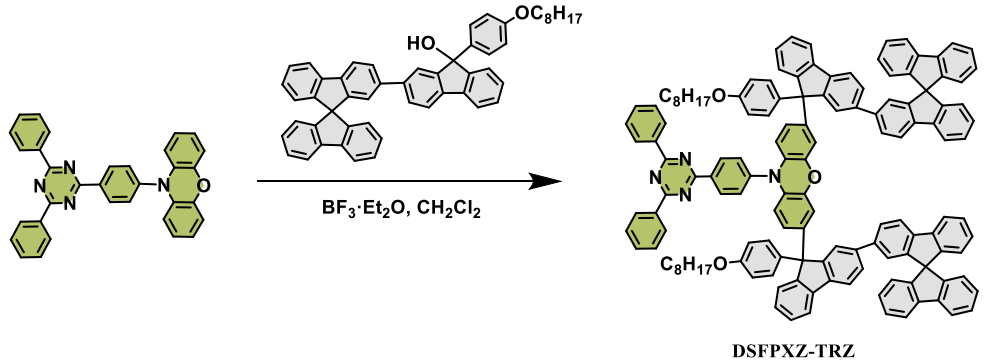

In a 500 mL two-necked round-bottomed flask charged with PXZ-TRZ (0.40 g，0.82 mmol), OHSBF (1.15 g, 1.64 mmol) and 250 mL of dry dichloromethane, a solution of

$BF_3 \cdot Et_2O$ (0.20 g，0.2 mL) in 50 mL dry dichloromethane was added dropwise. The reaction mixture was stirred at room temperature for 12 h. Water (100 mL) was added to quench the reaction. The mixture was separated and the aqueous phase was extracted with dichloromethane. The combined organic layers were washed with brine and dried over $MgSO_4$. After removal of the solvent, the crude product was purified by flash column chromatography using an eluent of petroleum ether: dichloromethane (4:1) to give a light yellow solid product DSFPXZ-TRZ (1.22 g，80%). 1H NMR (400 MHz, $CDCl_3$) δ 8.99 – 8.72 (m, 5H), 7.83 (td, *J* = 9.7, 8.7, 4.3 Hz, 7H), 7.61 (ddd, *J* = 13.6, 11.1, 6.9 Hz, 8H), 7.52 (dt, *J* = 8.0, 1.6 Hz, 2H), 7.48 – 7.39 (m, 3H), 7.40-7.28 (m, 9H), 7.21 (t, *J* = 7.4 Hz, 2H), 7.12-7.04 (m, 8H), 6.89 (d, *J* = 1.7 Hz, 2H), 6.78-6.65 (m, 8H), 6.47 (dd, *J* = 6.8, 2.0 Hz, 1H), 6.38 (ddd, *J* = 8.5, 3.6, 2.2 Hz, 1H), 5.82 (dd, *J* = 8.4, 1.4 Hz, 2H), 3.84 (t, *J* = 6.5 Hz, 3H), 1.71 (t, *J* = 7.3 Hz, 4H), 1.56 (s, 7H), 1.40 (dd, *J* = 14.1, 6.5 Hz, 4H), 1.34-1.21 (m, 21H), 0.92 – 0.82 (m, 9H). ^{13}C NMR (101 MHz, $CDCl_3$) δ 171.79, 157.83, 151.86, 149.25, 149.18, 148.65, 141.74, 141.34, 141.08, 140.92, 140.51, 139.43, 139.06, 136.94, 136.02, 132.69, 132.27, 131.47, 130.87, 129.05, 128.98, 128.70, 127.83, 127.74, 127.70, 127.60, 127.34, 127.12, 126.62, 125.87, 124.36, 124.14, 123.95, 122.60, 120.15, 120.09, 119.99, 115.53, 114.05, 112.72, 67.82, 65.98, 63.95, 31.80, 29.34, 29.27, 29.23, 26.05, 22.65, 14.12. MALDI-TOF-MS: m/z calcd for $C_{137}H_{106}N_4O_3$ $[M]^+$:1856.83, found: 1856.42.

S2. NMR spectra and mass spectra

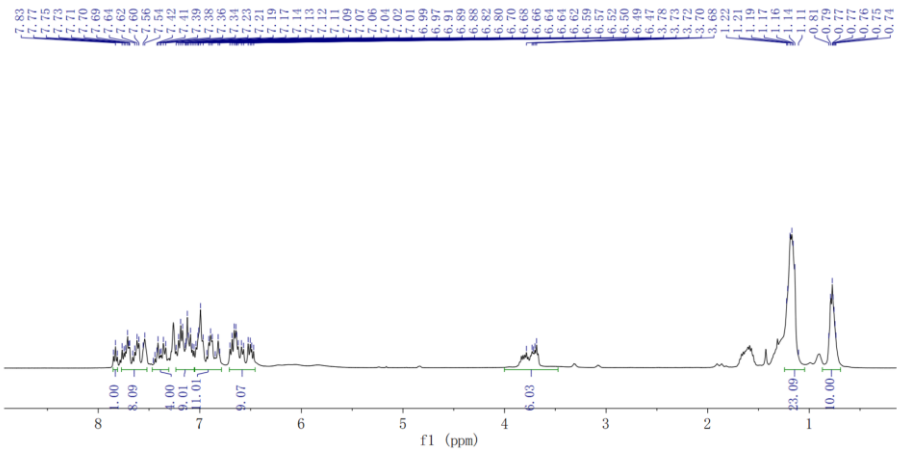

Figure S1. ^{1}H NMR spectrum of AG-EtPXZ.

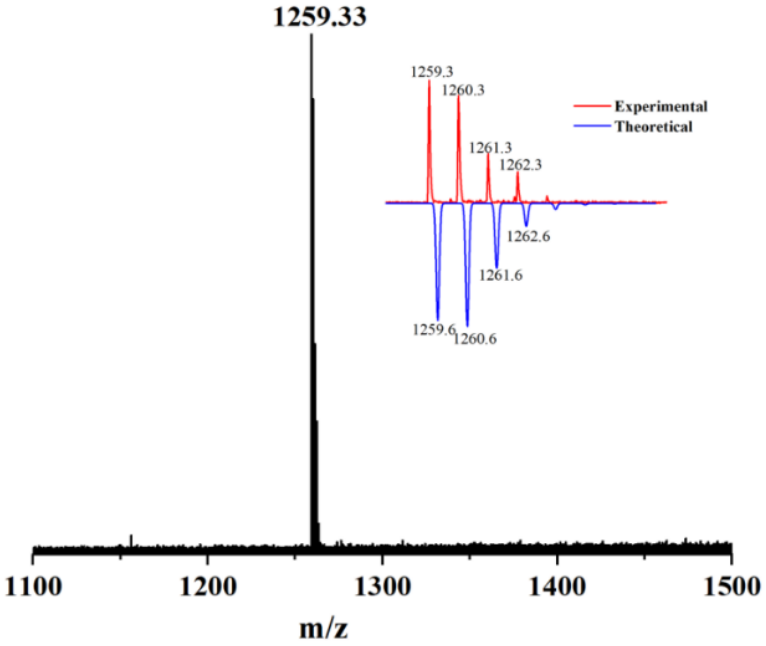

Figure S2. MALDI-TOF-MS spectrum of AG-EtPXZ.

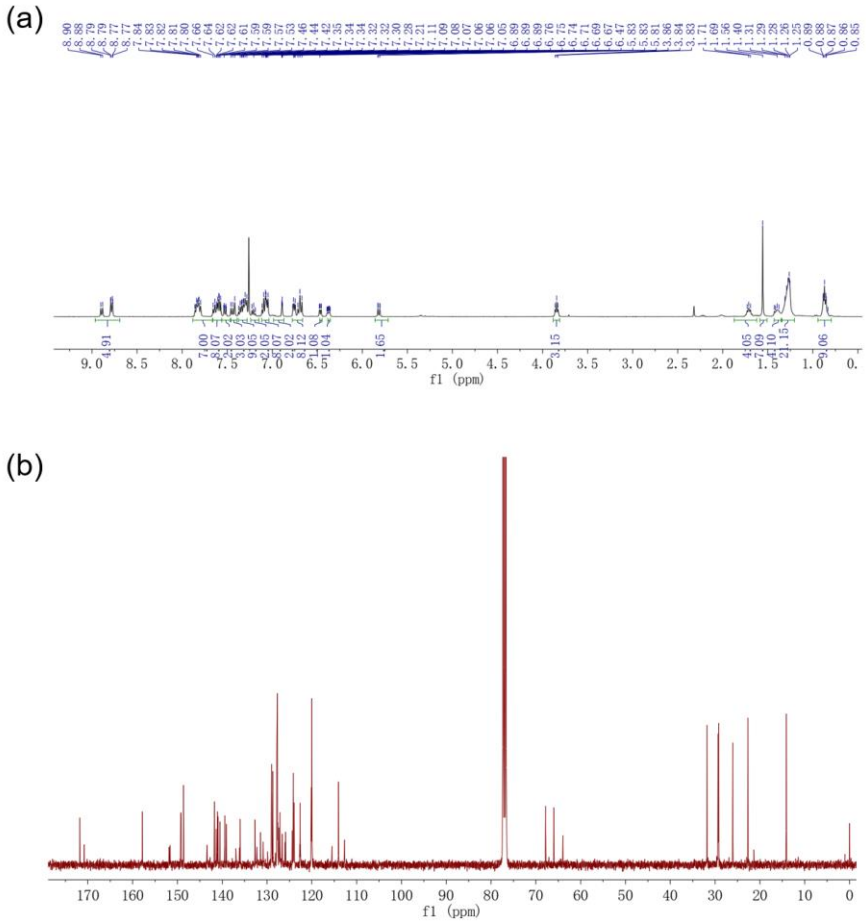

Figure S3. (a) ^{1}H NMR spectrum and (b) ^{13}C NMR spectrum of DSFPXZ-TRZ.

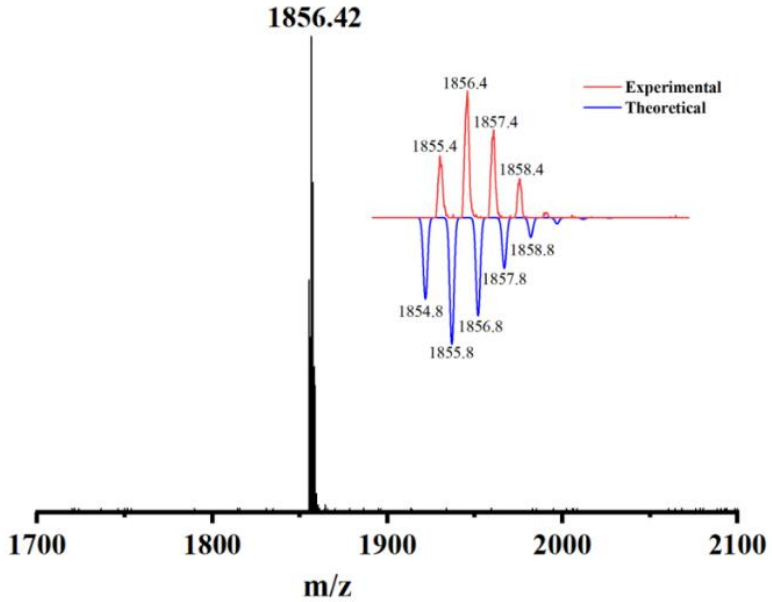

Figure S4. MALDI-TOF-MS spectrum of DSFPXZ-TRZ.

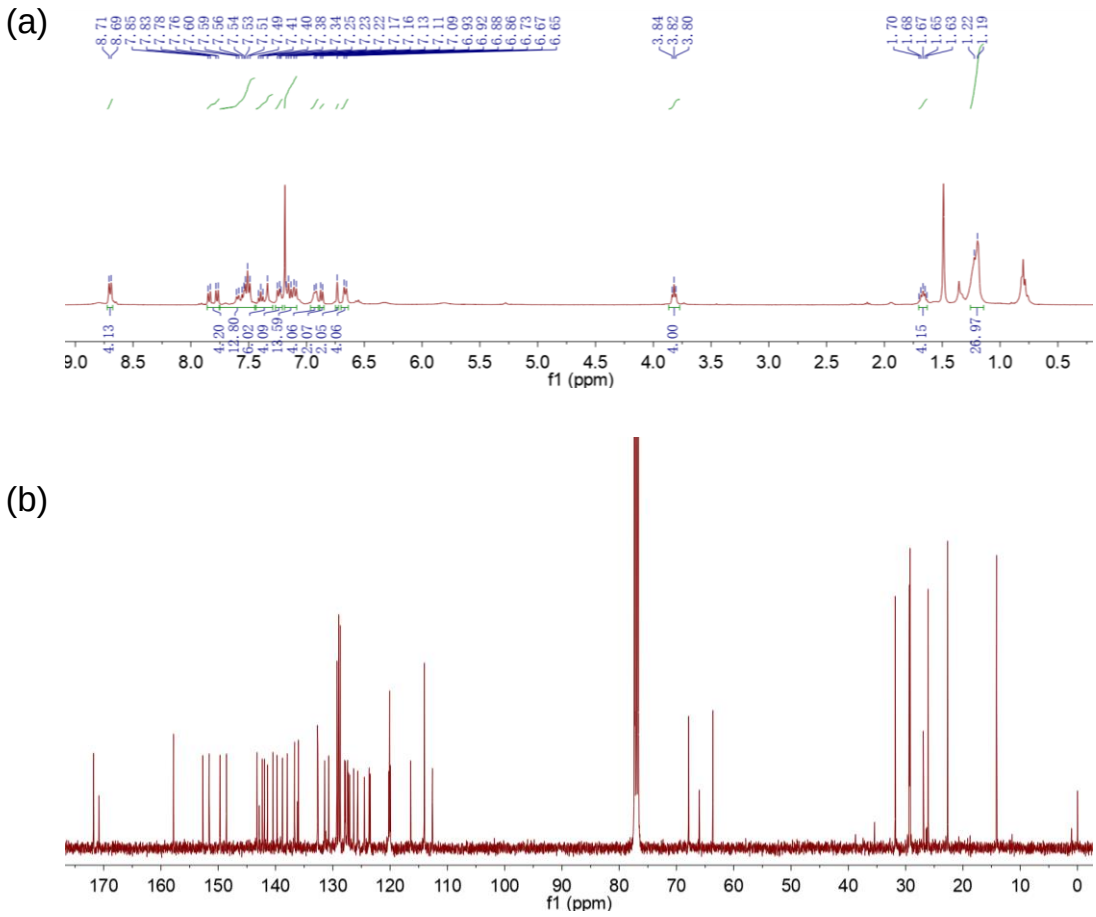

Figure S5. (a) ^{1}H NMR spectrum and (b) ^{13}C NMR spectrum of AG-PXZ- TRZ.

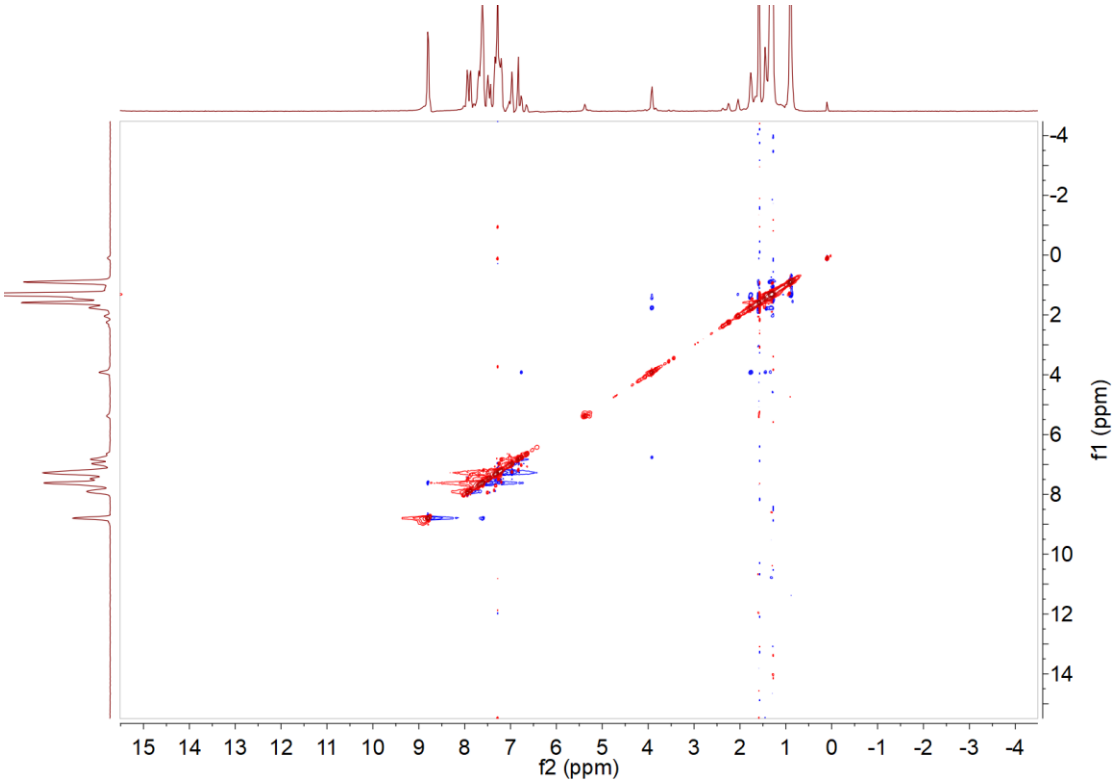

Figure S6. ^{1}H-^{1}H NMR NOESY spectrum of AG-PXZ- TRZ.

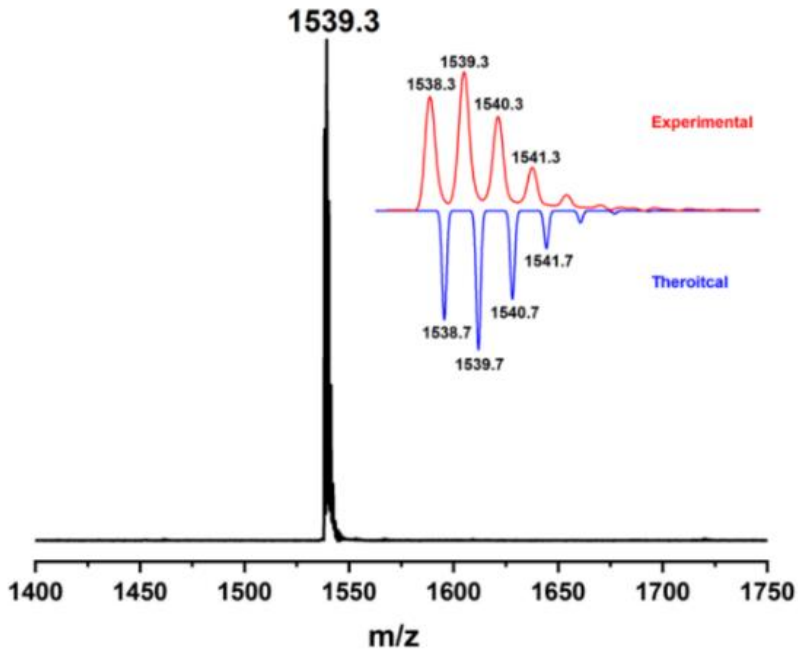

Figure S7. MALDI-TOF-MS spectrum of AG-PXZ- TRZ.

S3. Thermal properties and electrochemical properties

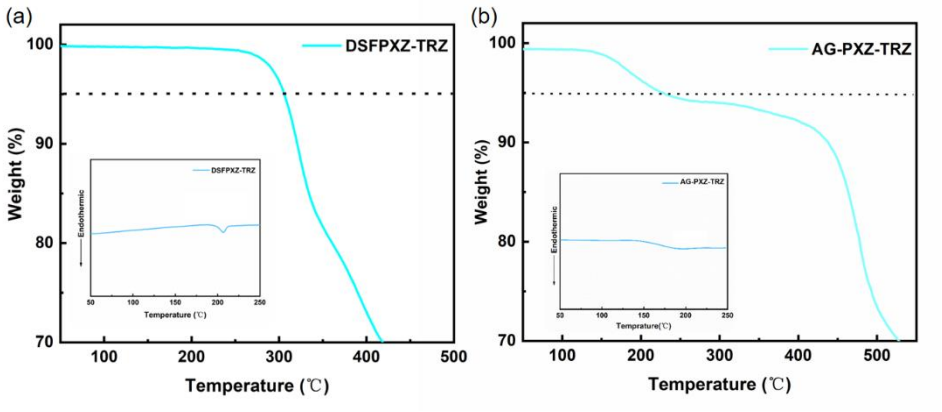

Figure S8. TGA and DSC curves of DSFPXZ-TRZ and AG-PXZ-TRZ.

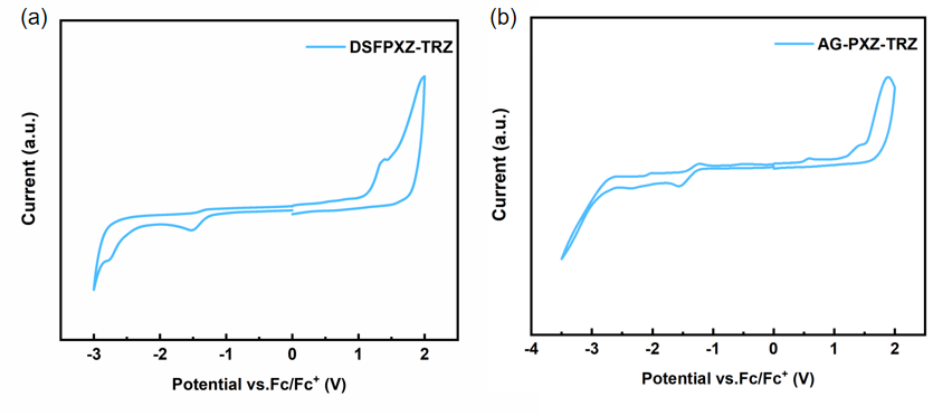

Figure S9. Cyclic Voltammetry (CV) curves of DSFPXZ-TRZ and AG-PXZ-TRZ in dichloromethane solution.

S4. Morphological properties

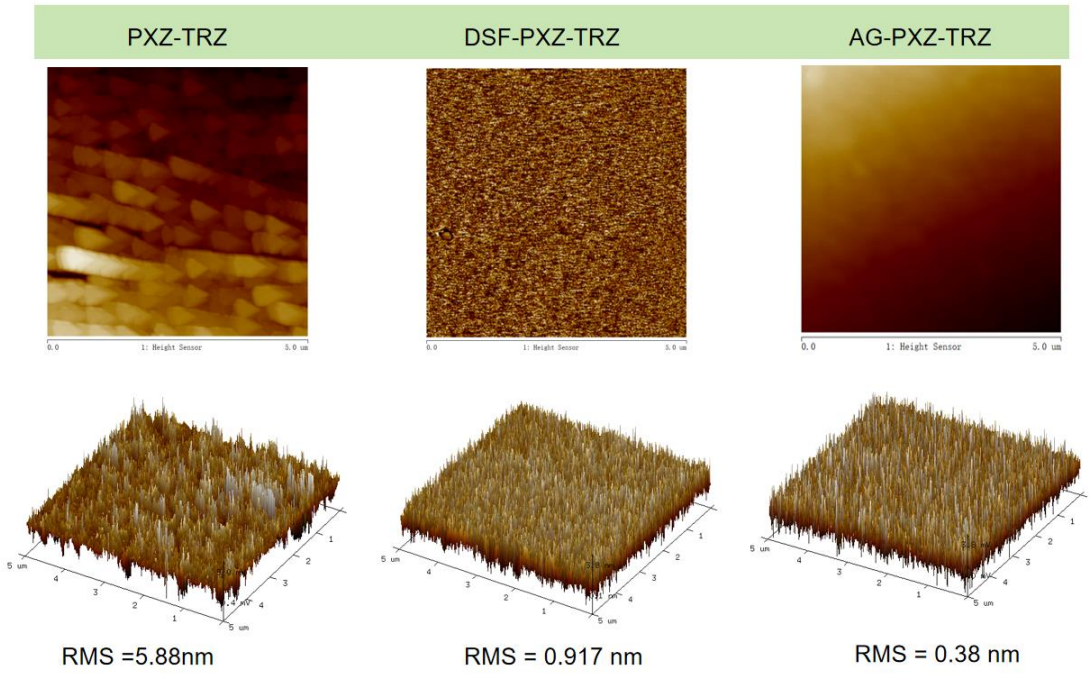

Figure S10. AFM topographic images of PXZ-TRZ, DSFPXZ-TRZ and AG-PXZ-TRZ.

S5. Photophysical properties

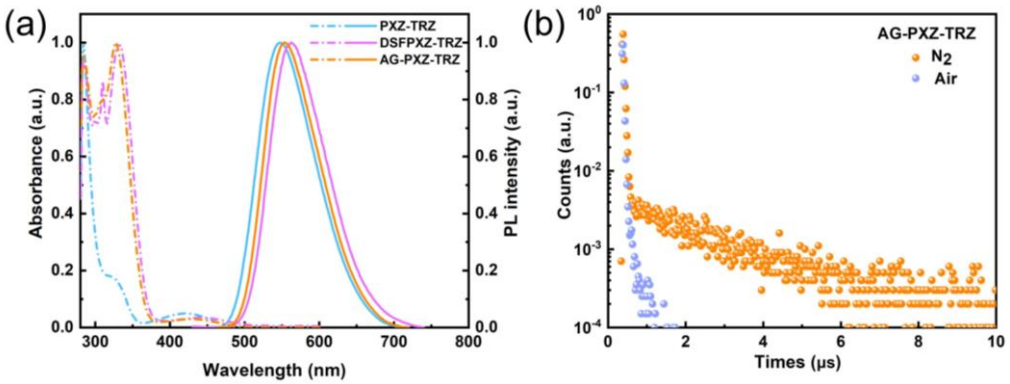

Figure S11. (a) Normalized UV–vis absorption and room temperature fluorescence (298 K) spectra in toluene (10−5 M). (b) AG-PXZ-TRZ in N_2 and air at 298 K in toluene solution.

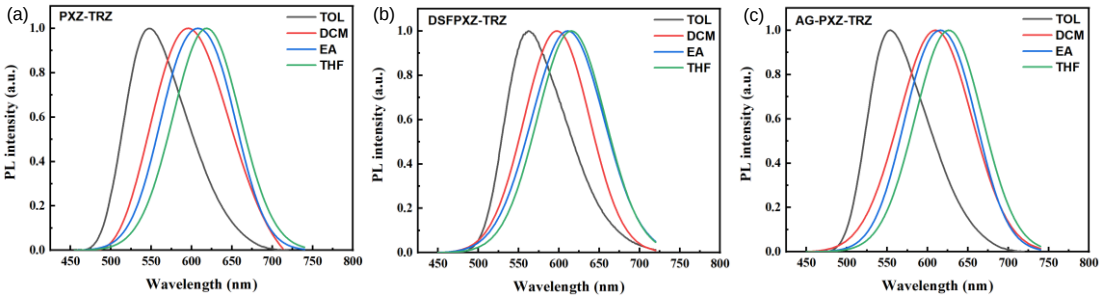

Figure S12. Normalized fluorescence spectra of (a) PXZ-TRZ, (b) DSFPXZ-TRZ, and (c) AG-PXZ-TRZ (10^{-5} M) in toluene, dichloromethane, ethyl acetate and tetrahydrofuran.

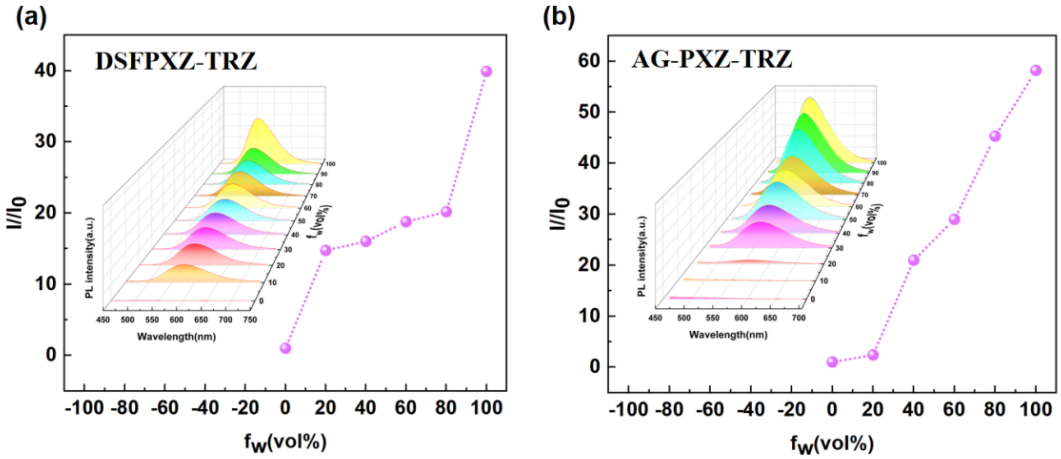

Figure S13. The PL intensity of DSFPXZ-TRZ and AG-PXZ-TRZ in Acetone/H_2O mixture (10^{-5} M) with different water fraction (f_w).

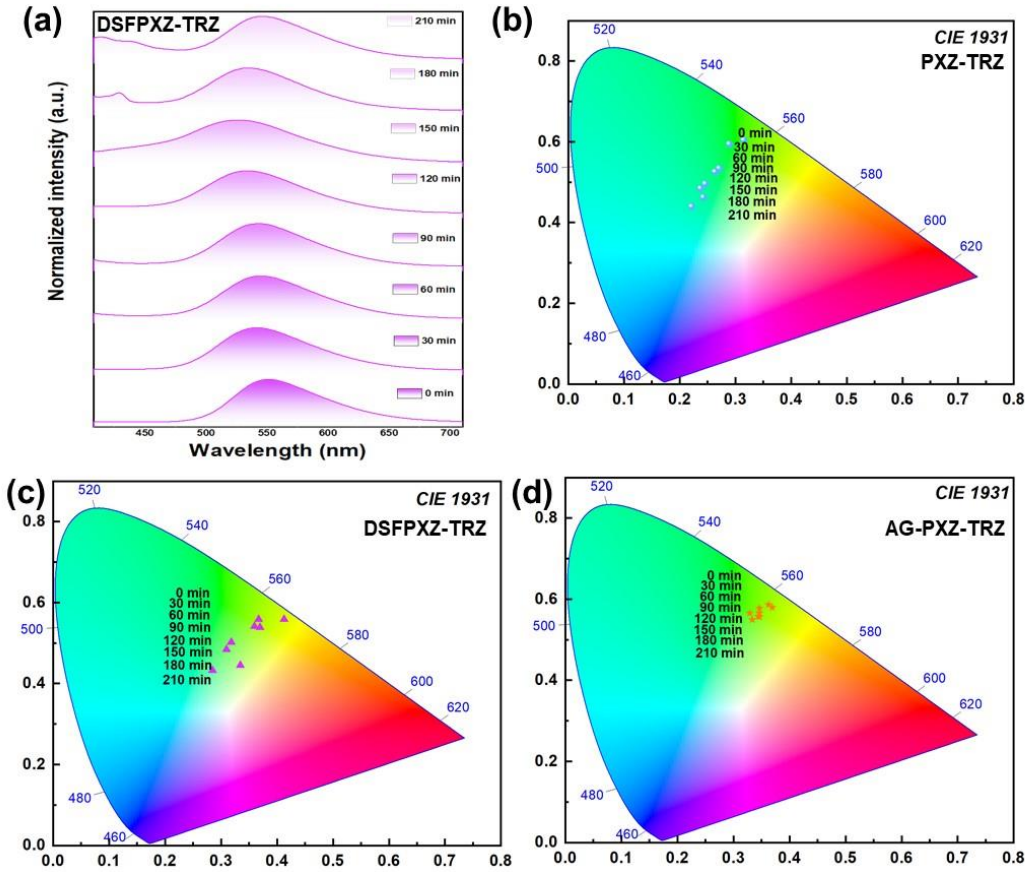

Figure S14. (a) PL spectra of the DSFPXZ-TRZ pristine films after various periods of ozone aging. The CIE 1931 color coordinates of (b) PXZ-TRZ, (c) DSFPXZ-TRZ, and (d) AG-PXZ-TRZ after various periods of ozone aging.

S6. Theoretical calculations

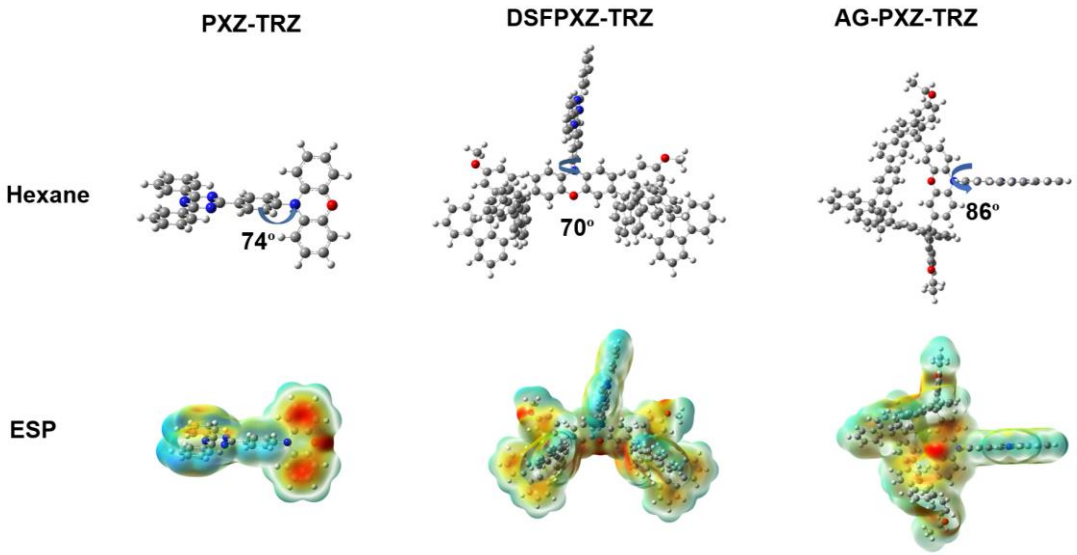

Figure S15. Molecular structure of PXZ-TRZ, DSFPXZ-TRZ and AG-PXZ-TRZ in hexane and electrostatic potential.

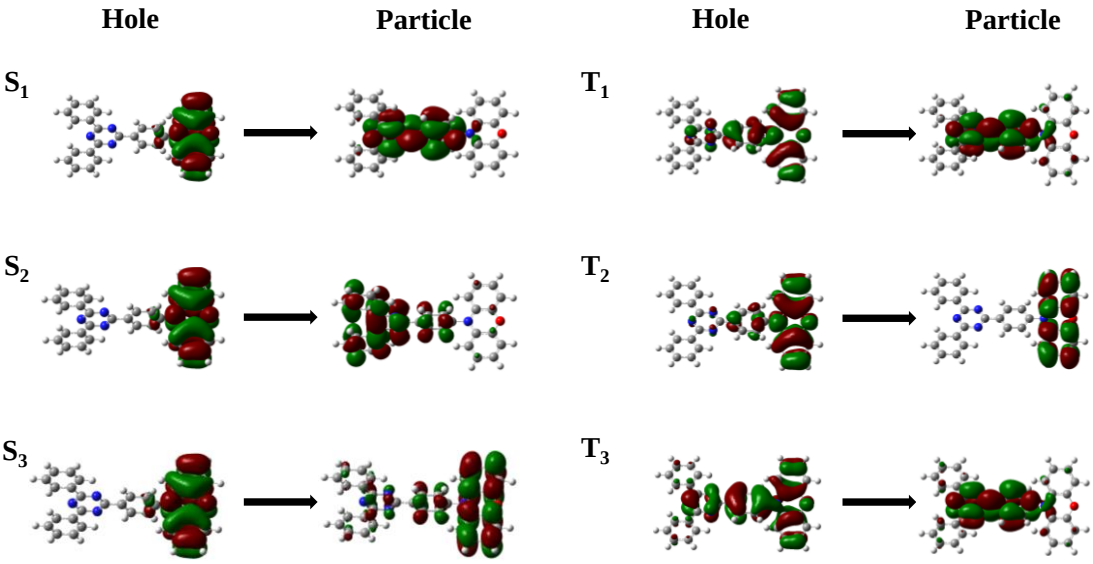

Figure S16. Natural transition orbitals (NTOs) of the S_1-S_3 and T_1-T_3 state for PXZ-TRZ molecule in n-hexane.

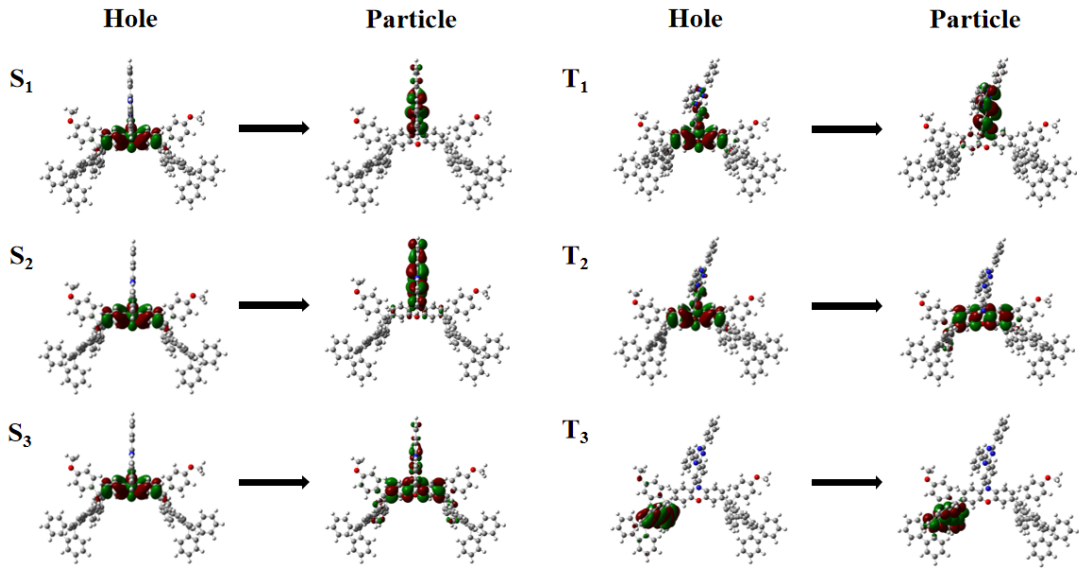

Figure S17. Natural transition orbitals (NTOs) of the S_1-S_3 and T_1-T_3 state for DSFPXZ-TRZ molecule in n-hexane.

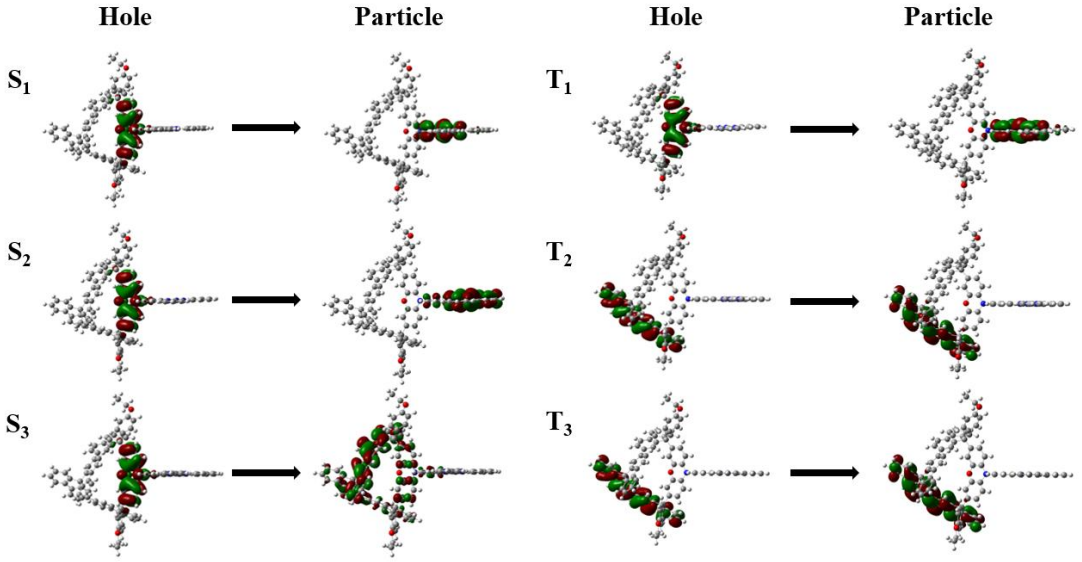

Figure S18. Natural transition orbitals (NTOs) of the S_1-S_3 and T_1-T_3 state for AG-PXZ-TRZ molecule in n-hexane.

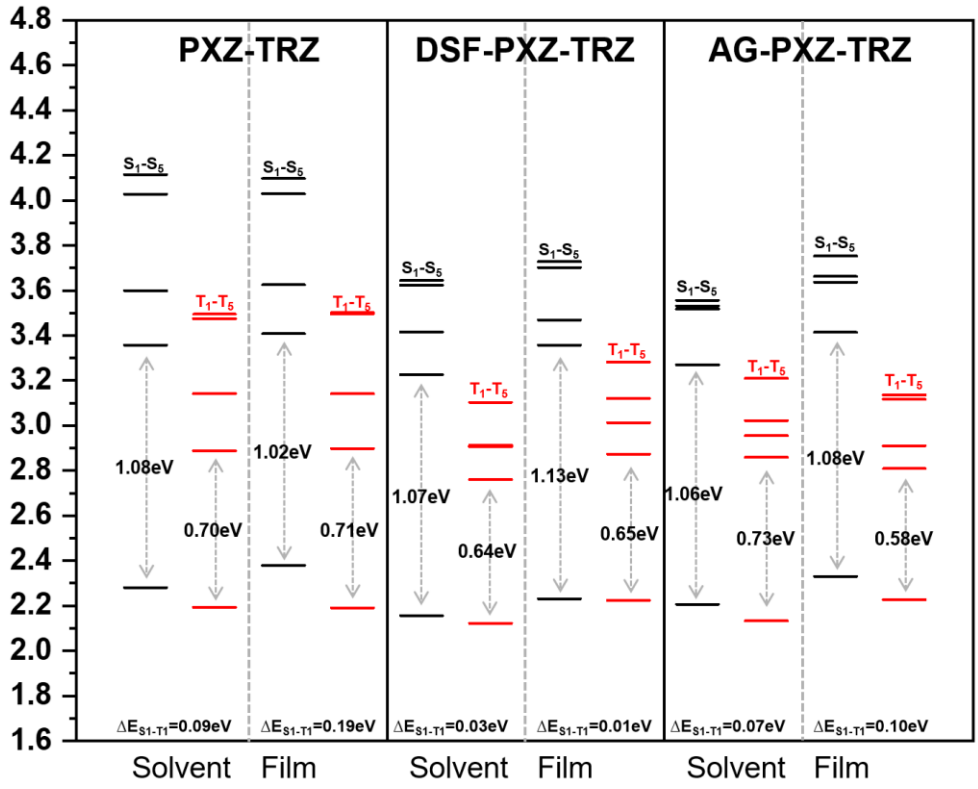

Figure S19. The first five adiabatic excitation energies for PXZ-TRZ, DSFPXZ-TRZ and AG-PXZ-TRZ in solvent and film, respectively.

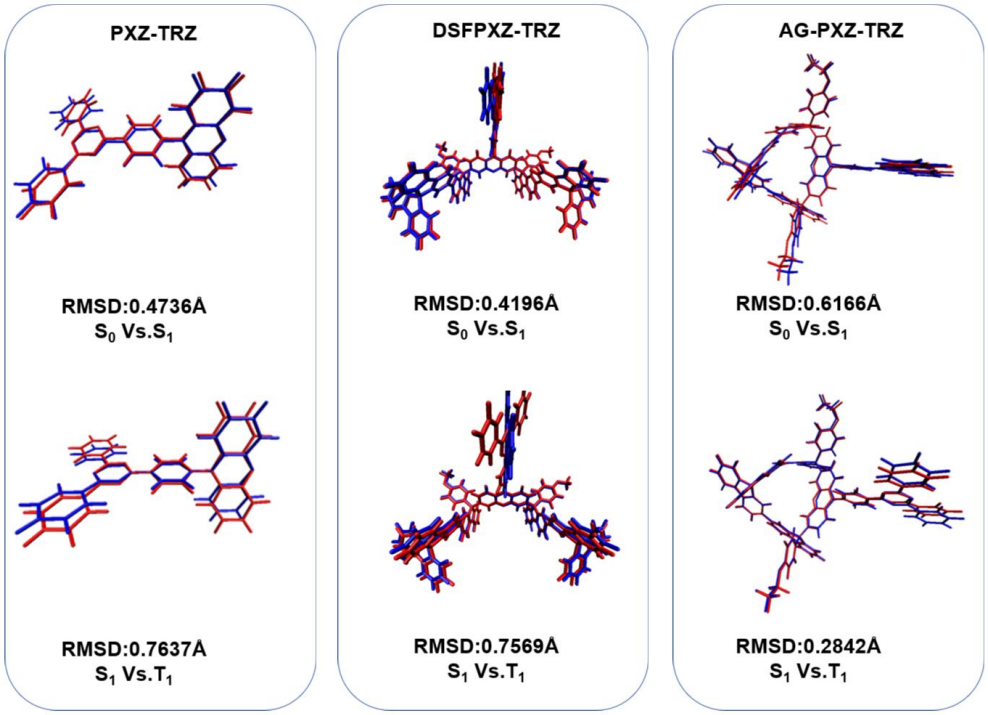

Figure S20. Geometry changes between S_0, S_1 and T_1 in n-hexane for PXZ-TRZ, DSFPXZ-TRZ and AG-PXZ-TRZ, respectively.

S7. Device performance

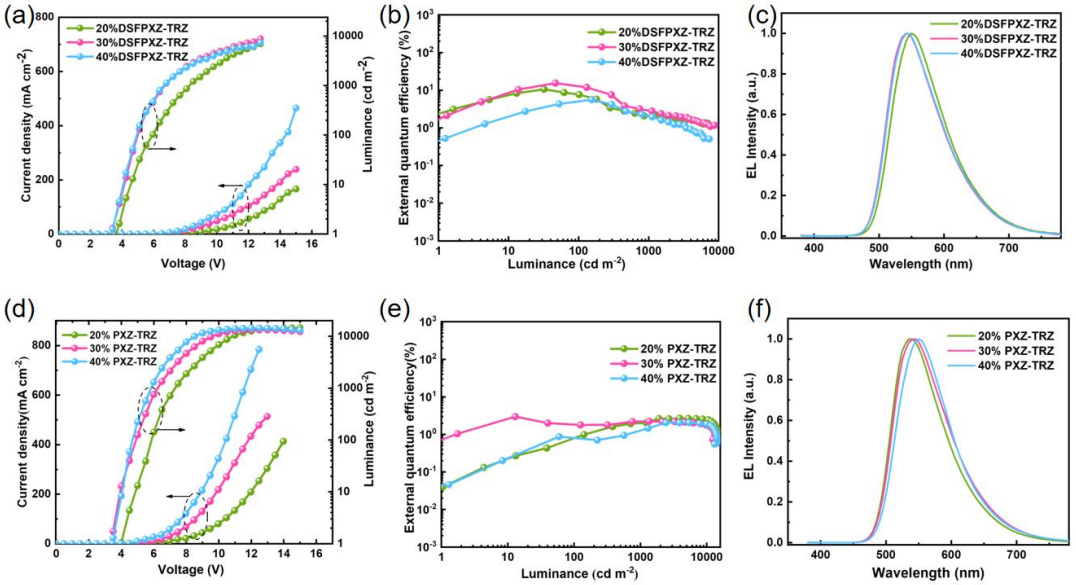

Figure S21. EL characteristic plots of devices employing DSFPXZ-TRZ and PXZ-TRZ at various doping concentrations. (a) and (d) current density and luminance vs driving voltage of DSFPXZ-TRZ and PXZ-TRZ, (b) and (e) external quantum efficiency vs luminance of DSFPXZ-TRZ and PXZ-TRZ, (c) and (f) EL spectra and of DSFPXZ-TRZ and PXZ-TRZ at various doping concentrations.

Table S1. EL performances of PXZ-TRZ, DSFPXZ-TRZ and PXZ-AG-TRZ based devices with different doping concentration.

EML	V_{on}(V)	L_{max}(cd/m^2)	CE_{max}(cd/A)	EQE_{max}(%)	λ(nm)	CIE
PXZ-TRZ	3.5	9032	1.84	0.65	555	(0.45, 0.54)
DSFPXZ-TRZ	3.5	4940	20.8	6.92	556	(0.45, 0.53)
PXZ-AG-TRZ	3	5897	32.1	10.4	552	(0.41, 0.56)
20% PXZ-TRZ	4	14600	8.78	2.69	536	(0.37, 0.58)
30% PXZ-TRZ	3.5	13365	7.20	2.97	544	(0.39, 0.56)
40% PXZ-TRZ	3.5	14371	6.70	2.05	549	(0.41, 0.56)
20% DSFPXZ-TRZ	4.5	6958	33.2	10.6	550	(0.42, 0.55)
30% DSFPXZ-TRZ	4	8758	46.7	15.4	542	(0.40, 0.56)
40% DSFPXZ-TRZ	4	7372	17.6	5.6	543	(0.40, 0.57)
20% AG-PXZ-TRZ	4	7352	57.5	18.1	550	(0.42, 0.54)
30% AG-PXZ-TRZ	4	12536	87.2	28.9	550	(0.41, 0.55)
40%AG-PXZ-TRZ	3	10433	22.4	6.92	550	(0.42, 0.55)

S8. References

[1] Tanaka, H.; Shizu, K.; Miyazaki, H.; Adachi, C., *Chem. Commun.* **2012,** *48*, 11392-11394.

[2] Yu, M.; Jia, X.; Lin, D.; Du, X.; Jin, D.; Wei, Y.; Xie, L.; Huang, W., *Front. Chem.* **2021,** *9*, 717892.

[3] Luo, W.; Wang, T.; Huang, Z.; Huang, H.; Li, N.; Yang, C., *Adv. Funct. Mater.* **2023,** 2310042.